**IMPACT STRENGTH OF RYUGU'S BOULDER INFERRED FROM METER-SIZED CRATER STATISTICS.** T. Morota[1,2*], S. Sugita[1,3], Y. Cho[1], E. Tatsumi[1,4,5], N. Sakatani[6], R. Honda[7], S. Kameda[6], M. Yamada[3], Y. Yokota[2], C. Honda[8], T. Kouyama[9], M. Matsuoka[2], M. Hayakawa[2], H. Sawada[2], K. Ogawa[2], H. Suzuki[10], K. Yoshioka[1], M. Kanamaru[2], M. Hirabayashi[11], T. Michikami[12], and Hayabusa2 team. [1]Univ. of Tokyo, Tokyo, Japan (morota@eps.s.u-tokyo.ac.jp), [2]JAXA, [3]Chiba Institute of Technology, [4]Dept. of Astrophysics, Univ. of La Laguna, [5]Instituto de Astrofisica de Canarias, [6]Rikkyo Univ., [7]Kochi Univ., [8]Univ. of Aizu, [9]AIST, [10]Meiji Univ., [11]Auburn Univ., [12]Kindai Univ.

**Introduction:** The proximity observations of asteroid Ryugu by Hayabusa2 showed that the asteroid has a spinning-top shape [1,2], numerous boulders [3, 4], and low bulk density [1], suggesting its rubble-pile structure [1]. Physical and chemical properties of these boulders may reflect the formation process of Ryugu's parent body [5] and aqueous alteration and thermal metamorphism in the parent body [3,6], and the collisional history from the parent body to Ryugu [7].

Cratering onto surfaces covered with large boulders, especially for Ryugu, Bennu, and Itokawa, may cause the "armoring effect", in which large boulders prevent meteoroid impactor penetration on the asteroid surface like armor [8–10]. Crater size influenced by the armoring effect depends on the impact strength of boulders. In order to obtain constraints on the impact strength of Ryugu's boulders, we investigated the size distributions of boulders and craters in diameter ranges from a few tens of centimeters to a few meters and 1 to 10 m, respectively, and quantified the armoring effect on Ryugu.

**Size Distributions of Boulders and Craters in the 1st Touchdown Area:** We performed size-frequency measurements of boulders in an area of about 2,000 $m^2$, including the 1st touchdown (TD1) site [11,12] using ONC high-resolution images (2–3 cm/pixel) obtained in the touchdown rehearsal operations. This region has low density of meter-sized boulders. Thus, it was selected as the primary landing site based on engineering safety criteria. The observed boulder size distribution follows a simple power law of $N_b(>D_b) = 0.0147\ D_b^{-2.2}$, where $D_b$ is the boulder diameter in km and $N_b(>D_b)$ is a number density of boulders $>D_b$ in $km^{-2}$.

We identified 11 crater candidates in an area of 3,700 $m^2$, including the boulder counting area (Fig. 1). The size distributions of craters identified using global mapping (0.5–2 m/pixel) and the crater search operation (CRA) data (~0.2 m/pixel) show the deficit of craters <100 m in diameter, suggesting that crater erasure processes have occurred on Ryugu's surface [3]. The observed size distribution of meter-sized craters in the TD1 area shows higher density than that extrapolated from the diameter range of 10–100 m in the global and CRA size distributions, which does not exhibit the effects by the crater erasure processes. However, the size distribution in the TD1 has a slightly flatter slope. We investigated whether or not this flatter slope can be explained by the armoring effect.

**Model Crater Size Distribution on Coarse-Grain Targets:** To construct the crater size-frequency model on the coarse-grain surface, we used the population model of main belt asteroids (MBAs) [13] and the crater scaling law for a coarse grain target [10]. On Ryugu, the size of impactors that produce meter-sized craters is estimated to be 1–10 cm. The population of asteroids in the size range is not understood. Therefore, we used a simple power-law relation fitted to the MBA population model in a diameter range of 1 to 10 m. The impact frequency was calculated using the intrinsic collision probability for MBAs [14].

Tatsumi & Sugita [10] found that the armoring effect can be classified into three regimes: (1) gravity scaled regime, (2) reduced size crater regime (armoring regime I), and (3) no apparent crater regime (armoring regime II). The armoring regime II occurs in the case that the impactor kinetic energy is less than the disruption energy of a target grain. We calculated model crater size distributions on a coarse-grain surface with a uniform grain size (Fig. 2). The figure shows that the crater diameter range in the armoring regime II becomes wider with increasing grain size, as expected. The model crater size distributions in the TD1 area were calculated by averaging the model size distributions on uniform grain surfaces with weights based on area fractions of each boulder size estimated from the observed boulder size distribution in the TD1 area. The derived model crater size distributions show that its slope becomes flatter with increasing the impact strength of boulders $Q^*$ (Fig. 3).

**Impact Strength of Boulders:** Figure 4 shows the model crater size distributions fitted to the size distribution of craters in the TD1 area. The observed size distribution slants down toward the left and can be well explained by the model size distributions for $Q^* >$ 1000 J/kg. The result that Ryugu's boulders have high impact strength despite its low static strength [15] is consistent with its high porosity [5,15]. Such pore-porous material is weaker in static strength, while higher porosity results in higher $Q^*$ because pores suppress the transmission efficiency of the impact energy throughout the body [16,17]. This may explain why Ryugu and

Bennu have such high abundance of boulders despite of their low thermal inertia.

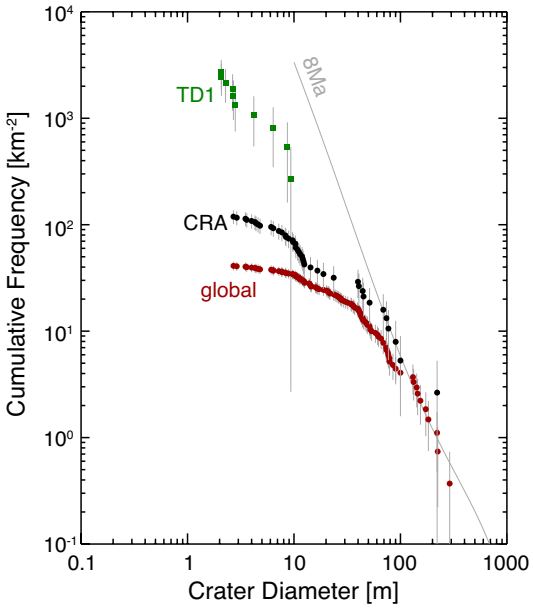


Figure 1. Cumulative crater size-frequency distribution. Global mapping and the Crater Search Operation (CRA) data are from Hirata et al. [18] and Cho et al. [19].

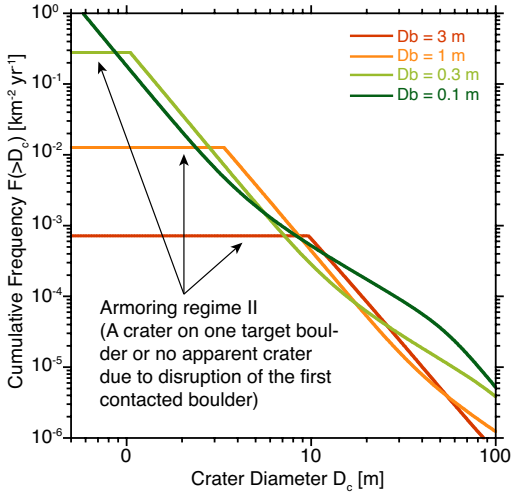


Figure 2. Model crater size distribution on coarse grains with an impact strength of 1000 J/kg.

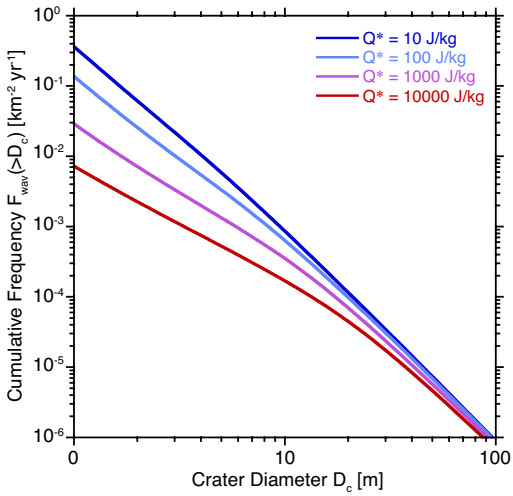


Figure 3. Model crater size distribution weighted by boulder area fraction.

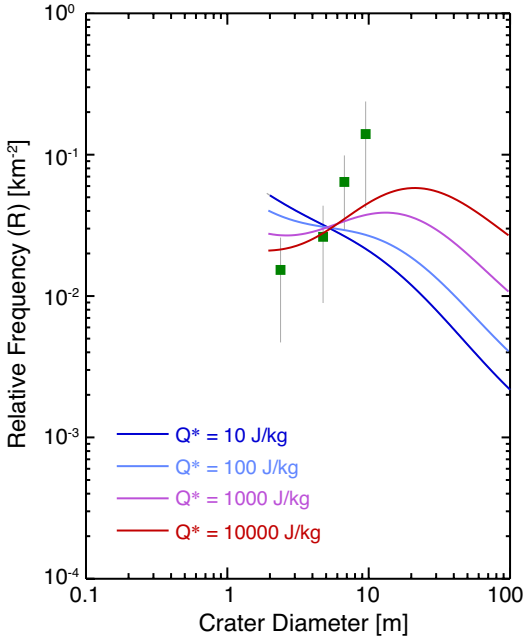


Figure 4. R-plot of craters in the TD1 area and model crater size distributions.

**Acknowledgments:** We used the software tool "craterstats" [20] to draw crater size-frequency distributions. T.M. thanks KAKENHI support from the JSPS (grant JP17K05633, JP17H06459, and JP19H01951). This study was also supported by JSPS Core-to-Core Program "International Network of Planetary Sciences". **References:** [1] Watanabe S. et al. (2019) *Science* 364, 268. [2] Hirabayashi M. et al. (2019) *AJL* 874, L10. [3] Sugita S. et al. (2019) *Science* 364, eaaw0422. [4] Michikami T. et al. (2019) *Icarus* 331, 179. [5] Okada T. et al. (2020) *Nature* 579, 518. [6] Kitazato K. et al. (2019) *Science* 364, 272. [7] Tatsumi E. et al. (2020) *Nature Astro.* doi:10.1038/s41550-020-1179-z. [8] Barnouin-Jha O.S. et al. (2005) *LPSC* 36, 1585. [9] Güttler C. et al. (2012) *Icarus* 220, 1040. [10] Tatsumi E. & Sugita S. (2018) *Icarus* 300, 227. [11] Morota T. et al. (2020) *Science* 368, 654. [12] Kikuchi S. et al. (2020) *SSR* 216, 116. [13] Bottke W.F. et al. (2005) *Icarus* 175, 111. [14] Bottke W.F. and Greenberg R. (1993) *GRL* 20, 879. [15] Grott M. et al. (2019) *Nature Astro.* doi: 10.1038/s41550-019-0832-x. [16] Love S.G. et al. (1993) *Icarus* 105, 216. [17] Nakamura A.M. et al. (2009) *PSS* 57, 111. [18] Hirata N. et al. (2020) *Icarus* 338, 113527. [19] Cho Y. et al. (2021) submitted. [20] Michael, G.G. & Neukum G. (2010) *EPSL*, *294*, 223–229.